Supporting Information

Terasawa et al. 10.1073/pnas.1120327109

SI Materials and Methods

Modeling of Shape Transformation. To determine whether the depletion volume effect can drive budding transformation, we evaluated the change of free energy due to the change in depletion volume ΔE_{dep} and bending energy ΔE_{bend} by approximating the shape before and after transformation as a spherocylinder (subscript sc) and two spheres (subscript ts), respectively. A spherocylinder has two geometrical parameters: the radius R_{sc} and length L_{sc} of the cylinder. Two spheres have only one geometrical parameter: the radius of two spheres R_{ts}. When these two shapes have the identical volume and surface area, the following relationships hold:

$$\text{Volume: } \frac{4}{3}\pi R_{\mathrm{sc}}^3 + \pi R_{\mathrm{sc}}^2 L_{\mathrm{sc}} = 2 \times \frac{4}{3}\pi R_{\mathrm{ts}}^3. \qquad \textbf{[S1]}$$

$$\text{Surface Area: } 4\pi R_{\mathrm{sc}}^2 + 2\pi R_{\mathrm{sc}} L_{\mathrm{sc}} = 2 \times 4\pi R_{\mathrm{ts}}^2. \qquad \textbf{[S2]}$$

In both equations, the terms in the left- and right-hand sides describe the quantities of a spherocylinder and two spheres, respectively. By equating [**S1**] and [**S2**], we derive the relationships of three geometrical parameters written as

$$R_{\mathrm{sc}} = (\sqrt{3} - 1)R_{\mathrm{ts}}. \qquad \textbf{[S3]}$$

$$L_{\mathrm{sc}} = 4R_{\mathrm{ts}}. \qquad \textbf{[S4]}$$

Next, we derive the depletion volume of these two shapes written as

$$V_{\mathrm{dep,sc}} = \left(\pi R_{\mathrm{sc}}^2 L + \frac{4}{3}\pi R_{\mathrm{sc}}^3\right) - \left(\pi (R_{\mathrm{sc}} - r_g)^2 + \frac{4}{3}(R_{\mathrm{sc}} - r_g)^3\right) \qquad \textbf{[S5]}$$

and

$$V_{\mathrm{dep,ts}} = 2 \times \frac{4}{3}\pi (R_{\mathrm{ts}}^3 - (R_{\mathrm{sts}} - r_g)^3), \qquad \textbf{[S6]}$$

where r_g is the gyration radius of the encapsulated polymer. From Eqs. **S3–S6**, we readily obtain the change of the depletion volume along with the shape transformation from the spherocylinder to two spheres:

$$\Delta V_{\mathrm{dep}} = V_{dep,sc} - V_{\mathrm{dep,ts}} = \frac{4}{3}\pi r_g^2 (3(2 - \sqrt{3})R_{\mathrm{ts}} - r_g). \qquad \textbf{[S7]}$$

The decrease of the energy due to this reduction of depletion volume is written as

$$\Delta E_{\mathrm{dep}} = \Delta \Pi \cdot \Delta V_{\mathrm{dep}}, \qquad \textbf{[S8]}$$

where $\Delta \Pi$ represents the difference in osmotic pressure between solutions in bulk and the depletion volume. Thus, we obtain the scaling relationship

$$|\Delta E_{\mathrm{dep}}| \propto \Delta \Pi \cdot r_g^2 R_{\mathrm{ts}}. \qquad \textbf{[S9]}$$

Next, we derive the difference in the bending energy of the membrane. The bending energy of a spherocylinder can be derived as the sum of the contributions of a cylinder and two semispherical caps, written as

$$E_{\mathrm{bend,sc}} = 8\pi\kappa_b + \pi\kappa_b \frac{L_{\mathrm{sc}}}{R_{\mathrm{sc}}}, \qquad \textbf{[S10]}$$

whereas that of two spheres is simply the sum of the bending energies of the two spheres;

$$E_{\mathrm{bend,ts}} = 2 \times 8\pi\kappa_b. \qquad \textbf{[S11]}$$

The change of bending energy along with the shape transformation is then obtained using Eqs. **S3** and **S4** as

$$\Delta E_{\mathrm{bend}} = E_{\mathrm{bend,sc}} - E_{\mathrm{bend,ts}} = 2\pi\kappa_b(3 - \sqrt{3}), \qquad \textbf{[S12]}$$

which is constant and independent of the vesicle size.

Using these equations, we can evaluate the change of the free energy from these contributions along with the shape transformation. We calculated the case of $R_{\mathrm{ts}} = 2.5$ µm (total volume and surface area are, respectively, 131 µm^3 and 157 µm^2) for the polymer-encapsulating conditions examined, and the results are summarized in Table S1. The osmolarity of the polymer-containing buffer was measured by an osmometer (OM-815; Biomedical Sciences, Inc.), and $\Delta\Pi$ was derived as the difference from the buffer without polymer.

Based on this theory, vesicles with a spherocylindrical shape spontaneously transform to a budded shape (two spheres) in conditions where $|\Delta E_{\mathrm{dep}}|$ is greater than $|\Delta E_{\mathrm{bend}}|$ ($|\Delta E_{\mathrm{bend}}| = 8.0 \times 10^{-19}$ J assuming $\kappa_b = 10^{-19}$ J). The selected results are plotted in Fig. 4*B* in the main text. Overall, the quantity of $|\Delta E_{\mathrm{dep}}|$ calculated is greater than $|\Delta E_{\mathrm{bend}}|$ in conditions with $P_{\mathrm{bud}}(v_{\mathrm{red}} = 0.7) > 0.1$ (budding occurred). This estimation proves that the depletion volume effect is the primary cause of vesicle transformation.

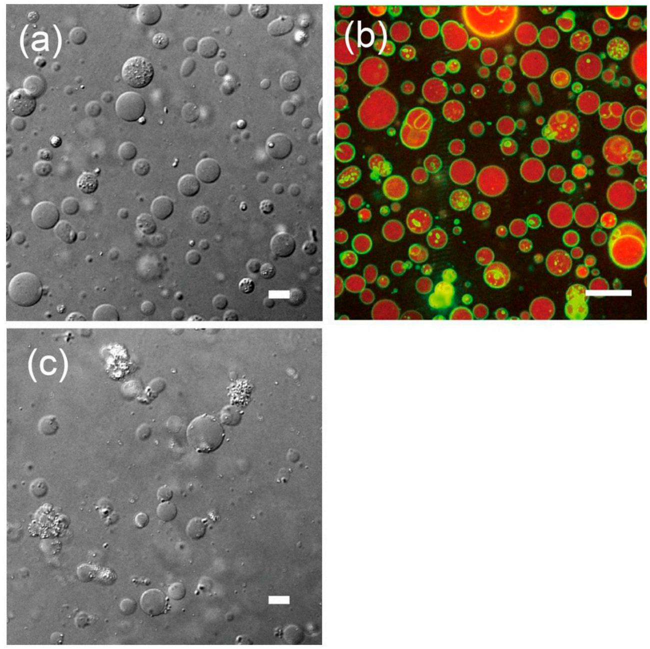

Fig. S1. (*A* and *B*) Differential interference contrast (DIC) and confocal micrographs of giant unilamellar vesicles formed by the W/O emulsion transfer method, which is composed of 1-palmitoyl-2-oleoyl-sn-glycero-3-phosphocholine (POPC), 1-palmitoyl-2-oleoyl-sn-glycero-3-[phospho-rac-(1-glycerol)] (POPG), and cholesterol. In the confocal image (*B*), green fluorescence represents the lipid membrane and is emitted from the BODIPY-HPC. Red fluorescence represents the inner aqueous phase of the giant vesicles and is emitted from the encapsulated fluorescent protein R-PE. Using this method, inner and outer solutions with defined composition and concentration were obtained, and the vesicles were determined to be mostly spherical and unilamellar. (*C*) DIC micrograph of vesicles composed of POPC/Chol. Without POPG, vesicles tended to aggregate, which made the experiments inefficient. (Scale bars: 10 μm.)

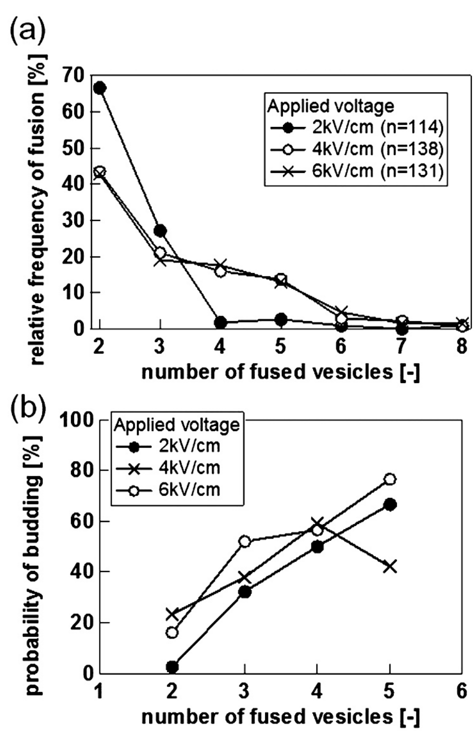

Fig. S2. (*A*) Relative frequency of the events versus the number of fused liposomes. The frequency of events in which four to five vesicles fuse together increases with electric voltage. (*B*) Probability of budding transformation versus the number of liposomes fused at various pulse voltages for electrofusion. Vesicles contain 3 mM PEG 6000.

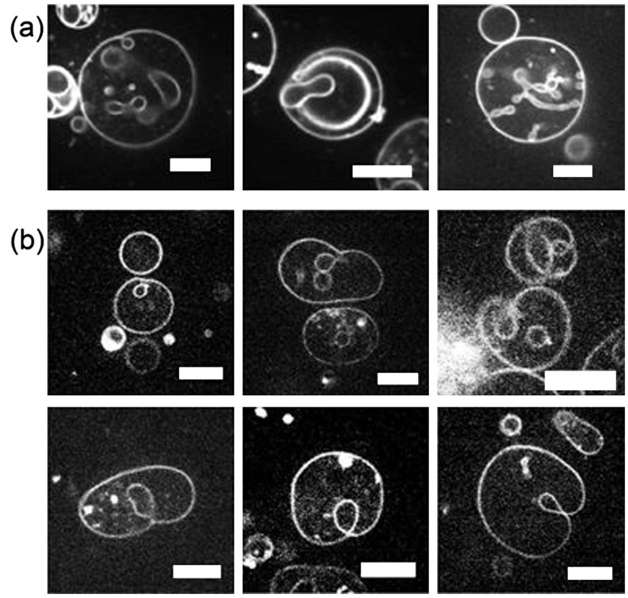

Fig. S3. Confocal images of vesicle shapes typically observed a few seconds after electrofusion. (Scale bar: 10 μm.) (*A*) Without PEG. Complex internal membrane structures were generated as a result of the vigorous fusion, whereas the outermost shape is almost spherical. (*B*) With 3 mM PEG 6000. Internal structures also appeared, but outermost shapes were various. They were mostly multivesicular, torus, or horseshoe shapes.

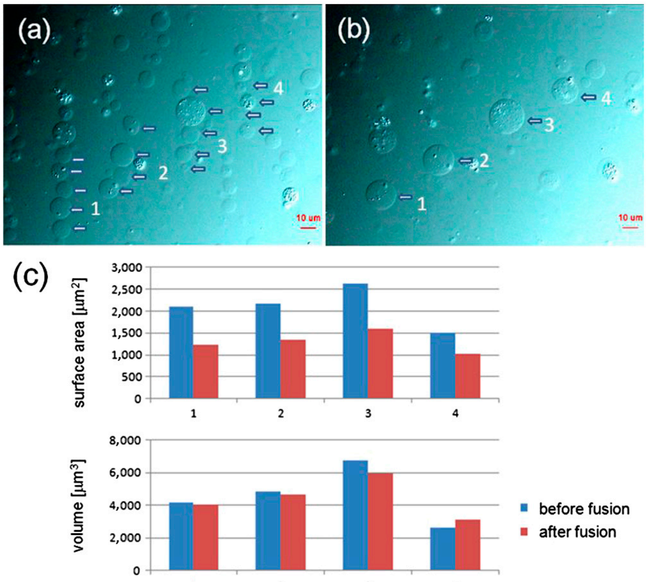

Fig. S4. Vesicle fusion without PEG. Microscope images before (*A*) and after (*B*) fusion. Vesicles indicated by arrows in *A* are those that fuse together to become single vesicles as indicated by arrows in *B*. (*C*) Total surface area and volume before and after fusion for vesicles indicated as 1–4 in the images. These quantities were calculated by assuming that all vesicles were spherical. The volume was conserved during fusion, whereas the surface area decreased by 30–40%. Excess membrane area invaginated into the vesicle to form a multivesicular structure (Fig. S3*A*).

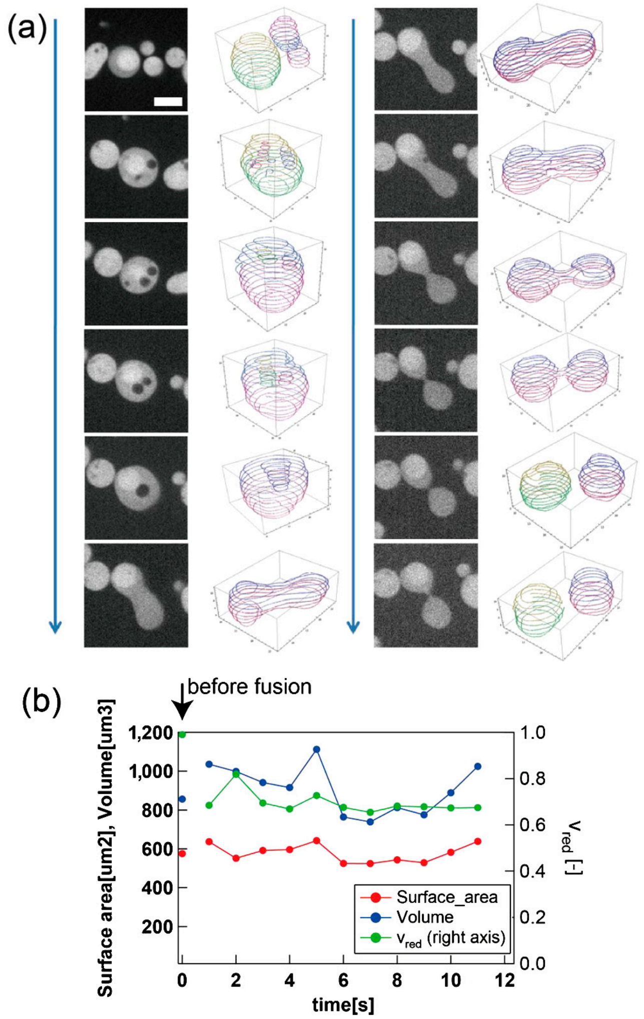

Fig. S5. (*A*) Time sequence (1-s interval) of shape transformation after electrofusion obtained by fluorescent confocal microscopy. (*Left*) Equatorial sections; inner volume was marked by fluorescent marker protein. (*Right*) Three-dimensional representation of vesicle edges extracted from images. (*B*) Time sequences of the volume and surface area. Surface area and volume were conserved during the fusion and after transformations within the CV of 7.7% and 13.3%, respectively.

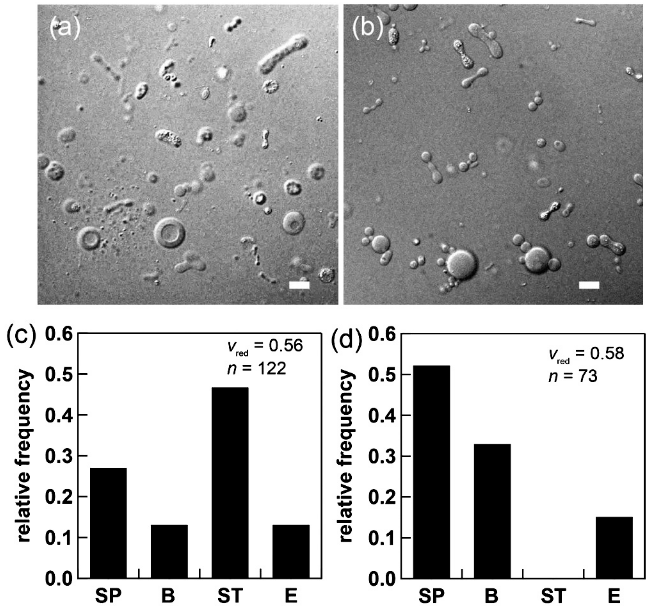

Fig. S6. Vesicle shapes under the hypertonic condition. (*A* and *B*) Differential interference contrast micrographs of vesicles not-containing and containing 3 mM PEG 20000, respectively. *Ca.* 1 M glucose solution was added to the vesicle suspension (1:1 volume ratio), which theoretically reduces the approximate 40% vesicle volume ($v_{red} \sim 0.6$). Vesicles were observed after approximately five to 10 min. (Scale bar: 10 μm.) (*C* and *D*) Relative frequencies of vesicle shapes without and with PEG, respectively, counted from 20 to 30 images. SP, B, ST, E respectively represent spherical, budded (dumbbell and pearl-chain-like shapes with distinct septa), stomatocyte (appeared as concentric double circles), and elongated (tubular and starfish-like) shapes. Without PEG (*C*), stomatocyte shape (ST) was dominant, in accordance with the theoretical prediction (1, 2). When containing PEG, budded shapes (*B*) became dominant, while stomatocyte shapes disappeared. Because depletion volume effect of encapsulated PEG induces positive curvature of the membrane, stomatocyte having negative curvature was energetically unfavorable. Budded shapes were instead favored due to the mechanism explained in the text (Fig. 2). Increased frequency of spherical vesicles (SP) was most likely due to the separated small vesicles after budding.

1. Seifert U, Berndl K, Lipowsky R (1991) Shape transformations of vesicles—phase-diagram for spontaneous-curvature and bilayer-coupling models. *Phys Rev A* 44:1182–1202.
2. Miao L, Seifert U, Wortis M, Dobereiner HG (1994) Budding transitions of fluid-bilayer vesicles—the effect of area-difference elasticity. *Phys Rev E Stat Nonlin Soft Matter Phys* 49:5389–5407.

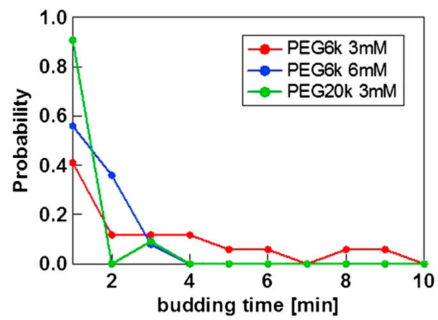

Fig. S7. Probability distribution of the time required for budding. When 3 mM PEG 6000 was encapsulated, the budding time varied from 1 to 10 min. In conditions with $C_{PEG\ 6000} = 6$ mM and $C_{PEG\ 20000} = 3$ mM, budding completed within 3 to 4 min.

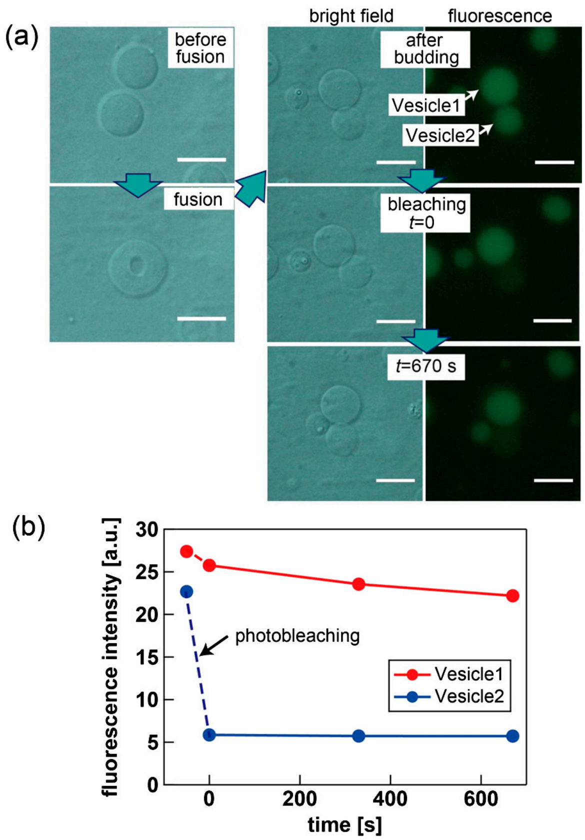

Fig. S8. Fluorescence recovery after photobleaching experiment. Vesicles contain 1.5 μM fluorescein conjugated BSA and 3 mM PEG 6000. (*A*) After budding transformation occurred, one of the daughter vesicles (vesicle 2) was photobleached ($t = 0$) by spot UV exposure. Even after approximately 10 min, the fluorescence intensity in the bleached vesicle did not recover, whereas that in the nonbleached vesicle remained constant (a slight decrease was observed due to bleaching from the excitation light). This result indicates that there was no transfer of internal aqueous content from the neighboring daughter vesicle.

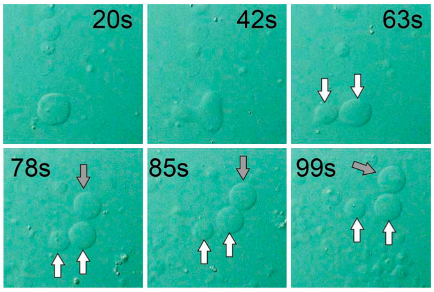

Fig. S9. Vesicles after budding transformation were occasionally separated by convectional flow. This time, sequence depicts the same data shown in Fig. 1*C*. Two white arrows indicate separated budded vesicles. A vesicle indicated by a gray arrow appeared from an off-focus plane around 70 s and has no relevance to the budded vesicles.

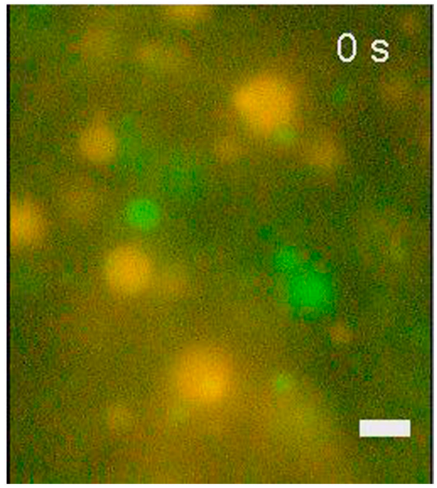

Movie S1. Epifluorescence observation of the electrofusion of GUVs. Time-lapse sequence with 1-s intervals is played at four frames/s (x4 play speed). Green (GFP) and orange (R-PE) fluorescent marker molecules encapsulated in GUVs rapidly mix after fusion. (Scale bar: 10 μm.)

Movie S1 (MOV)

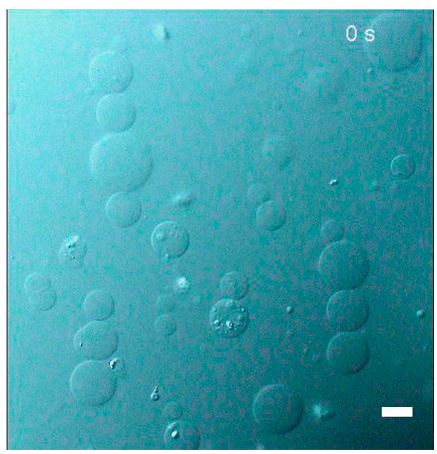

Movie S2. Differential interference contrast observation of the electrofusion of GUVs without PEG 6000. Time-lapse sequence with 1-s intervals is played at four frames/s (x4 play speed). Vesicle shape becomes spherical after fusion. (Scale bar: 10 μm.)

Movie S2 (MOV)

Movie S3. Differential interference contrast observation of the fusion to budding transformation of GUVs containing 5%wt/wt PEG 6000. Time-lapse sequence with 1-s intervals is played at four frames/s (x4 play speed). (Scale bar: 10 μm.)

Movie S3 (MOV)

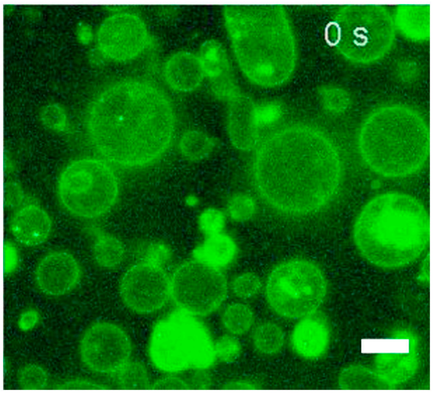

Movie S4. Epifluorescence observation of the fusion to budding transformation of GUVs containing 2.5%wt/wt PEG 6000. Time-lapse sequence with 1-s intervals is played at four frames/s (x4 play speed). Lipid membrane is illuminated by the fluorescence-tagged lipid (BODIPY-HPC). (Scale bar: 10 μm.)

Movie S4 (MOV)

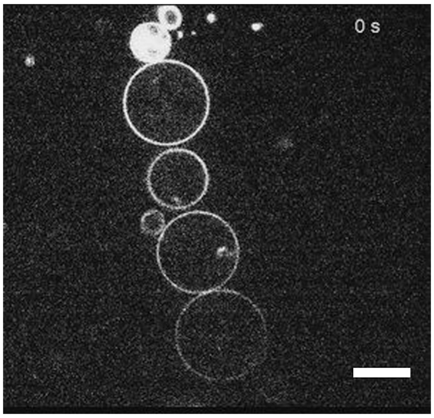

Movie S5. Confocal fluorescence observation of the fusion to budding transformation of GUVs containing 2.5%wt/wt PEG 6000. Time-lapse sequence with 20-s intervals is played at two frames/s (x40 play speed). The lipid membrane was illuminated by the fluorescence-tagged lipid (BODIPY-HPC). (Scale bar: 10 μm.)

Movie S5 (MOV)

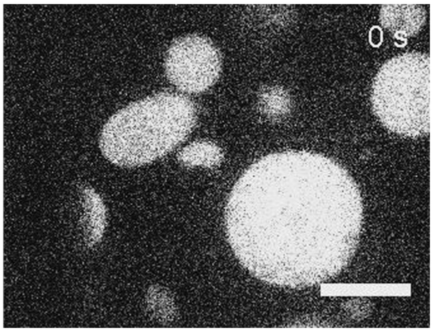

Movie S6. Confocal fluorescence observation of the fusion to budding transformation of GUVs containing 2.5%wt/wt PEG 6000. Time-lapse sequence with 20-s intervals is played at two frames/s (x40 play speed). The internal aqueous phase was illuminated by the fluorescence-tagged protein (FITC-BSA) encapsulated. (Scale bar: 10 μm.)

Movie S6 (MOV)

Movie S7. Differential interference contrast observation of the fusion to budding transformation of GUVs formed by the natural swelling method containing 5%wt/wt PEG 6000. Time-lapse sequence with 1-s intervals is played at four frames/s (x4 play speed). (Scale bar: 10 μm.)

Movie S7 (MOV)

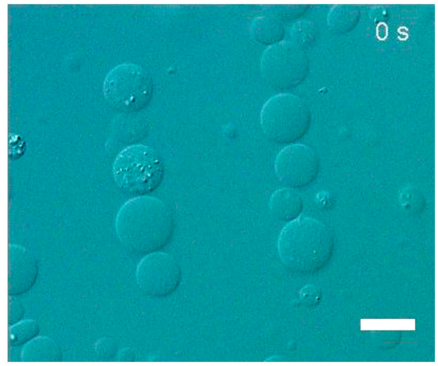

Movie S8. Differential interference contrast observation of the fusion to budding transformation of GUVs containing 3 mM PEG 20000. Time-lapse sequence with 1-s intervals is played at four frames/s (x4 play speed). (Scale bar: 10 μm.)

Movie S8 (MOV)

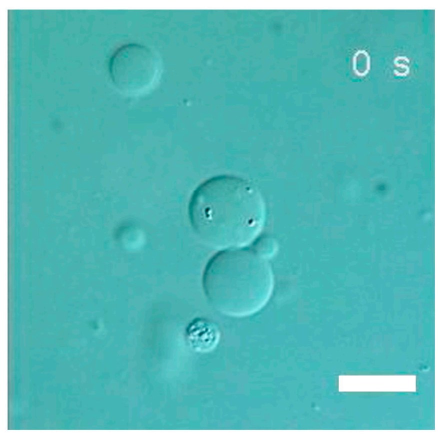

Movie S9. Differential interference contrast observation of repeated cycles of fusion to budding transformation containing 3 mM PEG 6000. Time-lapse sequence with 1-s intervals is played at four frames/s (x4 play speed). (Scale bar: 10 μm.)

Movie S9 (MOV)

Table S1. ΔE_{dep} estimated for experimental conditions tested

	Gyration radius,* nm	Polymer conc, mM	Osmolarity,† mOsm	$\Delta\Pi$, J/m^3	ΔV_{dep}, m^3	ΔE_{dep}, J
Buffer	—	0	642	—	—	—
PEG 400	0.69	3	645	7.40×10^{3}	3.89×10^{-24}	2.88×10^{-20}
		62	806	4.05×10^{5}		1.57×10^{-18}
PEG 6000	3.19	0.3	644	5.55×10^{3}	8.55×10^{-23}	4.75×10^{-19}
		1.5	674	7.81×10^{4}		6.68×10^{-18}
		3	708	1.64×10^{5}		1.40×10^{-17}
		6	830	4.63×10^{5}		3.96×10^{-17}
PEG 20000	4.95	1.25	724	2.05×10^{5}	2.06×10^{-22}	4.16×10^{-17}
		3	914	6.72×10^{5}		1.38×10^{-16}
DEX-6000	2.56	3	664	5.43×10^{4}	5.47×10^{-23}	2.97×10^{-18}
DEX-25000	4.97	3	747	2.61×10^{5}	2.07×10^{-22}	5.39×10^{-17}
DEX-50000	6.85	1.5	747	2.60×10^{5}	3.94×10^{-22}	1.02×10^{-16}

*The gyration radius of PEG and Dextran was calculated using the equations reported in refs. 1 and 2, respectively.
†Osmolarity was measured using an osmometer (OM-815; Biomedical Sciences, Inc.).

1. Kawaguchi S, et al. (1997) Aqueous solution properties of oligo-and poly(ethylene oxide) by static light scattering and intrinsic viscosity. *Polymer* 38:2885–2891.
2. Fishman ML, et al. (1987) Evaluation of root-mean-square radius of gyration as a parameter for universal calibration of polysaccharides. *Carbohydr Res* 160:215–225.